

1 **KDM5 inhibition offers a novel therapeutic strategy for the treatment of *KMT2D***
2 **mutant lymphomas**

3 James A Heward^{1*}, Lola Konali^{1*}, Annalisa D'Avola², Karina Close¹, Alison
4 Yeomans², Martin Philpott³, James Dunford³, Tahrima Rahim¹, Ahad F Al Seraihi¹, Jun
5 Wang¹, Koorosh Korfi¹, Shamzah Araf¹, Sameena Iqbal¹, Findlay Bewicke-Copley¹,
6 Emil Kumar¹, Darko Barisic⁴, Maria Calaminici¹, Andrew Clear¹, John Gribben¹, Peter
7 Johnson², Richard Neve⁵, Jessica Okosun¹, Udo Oppermann³, Ari Melnick⁴, Graham
8 Packham², Jude Fitzgibbon¹

9

10 **Author Affiliations:** 1 *Haemato-Oncology, Barts Cancer Institute, Charterhouse*
11 *Square, London, EC1M 6BQ, United Kingdom. 2 Cancer Research UK Centre, Cancer*
12 *Sciences, Faculty of Medicine, University of Southampton, Southampton General*
13 *Hospital, Southampton, SO16 6YD, United Kingdom. 3 Nuffield Department of*
14 *Orthopaedics, Rheumatology and Musculoskeletal Sciences, University of Oxford, OX3*
15 *7LD, United Kingdom. 4 Weill Cornell Medicine, New York, NY 10021 USA.*
16 *5 Gilead Sciences, Foster City, CA 94404, United States.*

17

18 ** These authors contributed equally to this article*

19

20 **Running title:** KDM5-inhibition in *KMT2D* mutant lymphoma

21

22 **Keywords:** Lymphoma, *KMT2D*, KDM5

23

24 **Additional information:**

25 **Financial support:** This work was supported by grants from Cancer Research UK
26 (15968 and C355/A26819 awarded to J.F. and 23669 awarded to G.P.) and the
27 Southampton Experimental Cancer Medicine and Cancer Research Centres. A.M. is
28 supported by NIH/NCI R35 CA220499, The Follicular Lymphoma Consortium, LLS
29 TRP 6572-19 and LLS SCOR 7021-20.

30

31 **Corresponding authors:** James Heward, Haemato Oncology, Barts Cancer Institute,
32 Charterhouse Square, London, EC1M 6BQ, United Kingdom. Phone: Tel: +44 (0)20
33 7882 8780, Email: J.A.Heward@qmul.ac.uk

34 Jude Fitzgibbon, Haemato Oncology, Barts Cancer Institute, Charterhouse Square,
35 London, EC1M 6BQ, United Kingdom. Phone: Tel: +44 (0)20 7882 3814, Email:
36 J.Fitzgibbon@qmul.ac.uk

37 **Conflicts of interest:** The authors declare no potential conflicts of interest. A.M.
38 receives research funding from Janssen and Sanofi, has consulted for Epizyme,
39 Constellation and Jubilant, and is an advisor to KDAC.

40 **Word count:** 5988

41 **Figure count:** 6 figures, 14 supplementary figures, 12 supplementary tables

42

43 **Abstract**

44 Loss-of-function mutations in *KMT2D* are a striking feature of the germinal centre (GC)
45 lymphomas, resulting in decreased H3K4 methylation and altered gene expression. We
46 hypothesised that inhibition of the KDM5 family, which demethylates H3K4me3/me2,
47 would re-establish H3K4 methylation and restore the expression of genes repressed
48 upon loss of *KMT2D*. KDM5-inhibition increased H3K4me3 levels and caused an anti-
49 proliferative response *in vitro*, which was markedly greater in both endogenous and
50 CRISPR-edited *KMT2D* mutant DLBCL cell lines, whilst tumour growth was inhibited
51 in *KMT2D* mutant xenografts *in vivo*. KDM5-inhibition reactivated both KMT2D-
52 dependent and -independent genes, resulting in diminished B-cell receptor signalling
53 and altered expression of BCL2 family members, including BCL2 itself, allowing it to
54 synergise with agents targeting these pathways. KDM5-inhibition may offer an
55 effective therapeutic strategy for ameliorating *KMT2D* loss-of-function mutations in
56 GC-lymphomas.

57 **Statement of significance**

58 We detail a novel way of reverting the effects of loss-of-function mutations in the
59 histone methyltransferase *KMT2D* by inhibiting the KDM5 demethylase family,
60 increasing levels of H3K4me3 and restoring expression of KMT2D regulated genes.

61

62 **Introduction**

63 Although epigenetic dysregulation is a feature of most cancers, few are as strikingly
64 dependent as GC-lymphomas. The vast majority of Follicular Lymphoma (FL) tumours
65 harbour loss-of-function mutations in *KMT2D* (80%) alongside mutations in *CREBBP*
66 (60%) and *EZH2* (25%) (1-4), with *KMT2D* also frequently mutated (30%) within the
67 GC B-cell (GCB) subtype of Diffuse Large B-cell Lymphoma (DLBCL) (5-7). The
68 majority of *KMT2D* mutations in GC-lymphomas are truncating, arise early during
69 tumour development, and are often bi-allelic (1,8-10), yet despite their frequency, no
70 therapies targeting these mutations have been reported.

71

72 The histone methyltransferase *KMT2D* (ENSG00000167548; formerly *MLL2* or *Mll4*)
73 is a member of the *KMT2* family of methyltransferases (*KMT2A-H*) which catalyse
74 the mono-, di- and tri-methylation of Histone 3 Lysine 4 (H3K4) (11). These
75 modifications are generally associated with active transcription, with H3K4me1
76 predominantly located at enhancers and H3K4me3 at active and poised promoters (12).
77 *KMT2D* has preferential mono-methyltransferase activity and deposits H3K4me1 at
78 enhancers, although it also acts as the central structural-component of the COMPASS-
79 like multi-protein complex and is required for the correct recruitment of other enzymes
80 including the histone acetyltransferases EP300/*CREBBP* and the H3K27me3
81 demethylase *KDM6A* (*UTX*) (13,14).

82

83 Loss of *Kmt2d* has been demonstrated to decrease H3K4me1/me2 deposition, alter gene
84 expression and to co-operate with *Bcl2* overexpression in *VavP-Bcl2* mice, increasing
85 proliferation within the GC and driving lymphomagenesis. Germline *KMT2D*
86 mutations are also the predominant cause of Kabuki syndrome, a developmental

87 disorder with defects in B-cell development but no apparent increase in GC-lymphoma
88 prevalence (15,16), highlighting that *KMT2D* mutations are likely to co-operate with
89 other lesions to cause GC-lymphomas.

90

91 H3K4 methylation levels are also regulated by the Lysine Specific Demethylase
92 (KDM) families LSD1 and KDM5, which demethylate H3K4me1 to H3K4me0 and
93 H3K4me3/me2 to H3K4me1 respectively. The KDM5 family utilises α -ketoglutarate
94 as a substrate and contains four members; *KDM5A (JARID1A/RBP2)*, *KDM5B*
95 (*JARID1B/PLU1*), *KDM5C (JARID1C/SMCX)* and *KDM5D (JARID1D/SMCY)*. The
96 KDM5 family has essential roles in regulating gene expression in a variety of contexts,
97 and although mutations of KDM5 genes are rare, KDM5A and KDM5B have been
98 implicated as potential therapeutic targets due to their upregulation in several cancers
99 (17) and apparent role as drivers of metastasis and drug resistance (18-20).

100

101 In this report, we hypothesised that KDM5-inhibition would re-establish H3K4
102 methylation and restore the expression of genes deregulated upon loss of *KMT2D*.
103 Using several different KDM5-inhibitors (KDM5i), we demonstrate that KDM5-
104 inhibition has strong anti-proliferative and cytotoxic activity on GCB-DLBCL cell
105 lines, likely through a combination of regulating BCR-signalling and the expression of
106 *BCL2* family members. Critically, KDM5-inhibition sensitivity appears to be
107 dependent on the presence of *KMT2D* mutations, suggesting that KDM5-inhibition may
108 offer a targeted therapy for *KMT2D* mutant GC-lymphomas.

109

110 **Results**

111

112 **KDM5-inhibition increases global H3K4me3 levels in GC-lymphoma cells**

113 To assess whether the KDM5 family was a suitable therapeutic target for GC-
114 lymphomas, we first quantified the expression of the four KDM5 isoforms (*KDM5A-*
115 *D*) in DLBCL cell lines, primary FL (ICGC (21)) and DLBCL (ICGC/TCGA) biopsies
116 and normal GC B-cells (BLUEPRINT (22)) (Figure 1a+b). *KDM5A* and *KDM5C* were
117 highly expressed in all the samples whilst expression of the Y-linked *KDM5D* was
118 restricted to male derived cell lines (Figure 1a). Protein expression was confirmed for
119 *KDM5A*, *KDM5C* and *KDM5D* by western blot analysis (Supplementary Figure 1a).

120

121 We then examined the effect of three individual KDM5i on H3K4 methylation; KDM5-
122 inh1 (Patent no. WO 2014/131777 A1 – EpiTherapeutics/Gilead (23)), Compound-48
123 (Constellation Pharmaceuticals (24)) and KDM5-C70 (25). All three KDM5i increased
124 H3K4me3, with KDM5-inh1 the most potent and Compound-48 and KDM5-C70
125 requiring concentrations around 10-fold higher to induce similar increases in H3K4me3
126 (Figure 1c). In GC-lymphoma cell lines, KDM5-inh1 induced time- and concentration-
127 dependent increases in H3K4me3, alongside modest decreases in H3K4me1/me2
128 (Figure 1d+e; Supplementary Figure 1b+c), without altering *KDM5A* and *KDM5C*
129 protein levels (Supplementary Figure 1d+e). KDM5-inh1 had no effect on histone
130 marks mediated by the two closest related KDM families, KDM4
131 (H3K9me3/H3K36me3) and KDM6 (H3K27me3) (17), indicating that KDM5-inh1 is
132 specific for KDM5 (Supplementary Figure 2a+b). KDM5-inhibition also increased
133 H3K4me3 in primary FL cell-suspensions (n=8), with H3K4me3 increased to a greater
134 degree in both *KMT2D* mutant cell lines and cell-suspensions, versus WT, at 48h
135 (Supplementary Figure 2c+d).

136

137 **KDM5-inhibition has selective cytostatic and cytotoxic activity on *KMT2D* mutant**
138 **cell lines**

139 We next examined the cytostatic effect of KDM5-inhibition on an extended panel of
140 cell lines. KDM5-inh1 had a varied impact upon proliferation after five days, with some
141 cell lines insensitive and others displaying strikingly low EC₅₀ values (e.g. OCI-LY-18
142 = 3nM, SU-DHL-6 = 10nM; Figure 2a+b; Supplementary Figure 3a). Compound-48
143 and KDM5-C70 were less potent, although reduced proliferation was observed in SU-
144 DHL-6 and OCI-LY-18, the cell lines most sensitive to KDM5-inh1 (Supplementary
145 Figure 3a). Grouping of the cell lines by *KMT2D* mutation status revealed that KDM5-
146 inh1 had a significantly greater anti-proliferative effect upon *KMT2D* mutant cell lines
147 (Mann-Whitney U, P value = 0.003; Figure 2b+c), with eight out of nine of the most
148 sensitive harbouring *KMT2D* mutations. The majority of cell lines examined (6/8)
149 displayed lower EC₅₀ values after 10 days of treatment than at five days (Supplementary
150 Figure 3b+c), indicating that KDM5-inhibition has sustained anti-proliferative activity
151 in lymphoma cells. Furthermore, quantification of DNA content and Annexin/7-AAD
152 staining indicated that the most sensitive cell lines were undergoing apoptosis following
153 KDM5-inhibition (Figure 2d; Supplementary Figure 3d-f).

154

155 **Inducing and correcting *KMT2D* mutations by CRISPR alters KDM5-inhibition**
156 **sensitivity**

157 Since *KMT2D* mutant cells were more sensitive to KDM5-inhibition than WT cells
158 (Figure 2b+c), we next tested whether inducing or correcting *KMT2D* mutations in cell
159 lines would alter KDM5-inhibition sensitivity. Using CRISPR we introduced *KMT2D*
160 mutations in two WT cell lines; WSU-DLCL2, the least sensitive t(14;18) positive cell

161 line and HT, the least sensitive cell line overall. Three WSU-DLCL2 clones (#8, #22,
162 #61; Supplementary Table 1) harbouring mono-allelic truncating mutations displayed
163 reduced proliferation following KDM5-inhibition (Figure 2e), with an average decrease
164 of 16% in area under the curve (AUC) values. Global levels of H3K4me3/me2/me1
165 appeared unaltered by *KMT2D* loss in untreated cells whilst KDM5-inhibition induced
166 similar increases in H3K4me3 in mutant and WT cells (Supplementary Figure 4a+b).
167 In contrast to WSU-DLCL2, the CRISPR-edited *KMT2D* mutant HT cells appeared
168 intrinsically resistant to KDM5-inhibition, with no consistent changes in proliferation
169 observed (Supplementary Figure 4c+d).

170

171 CRISPR was also employed to correct the homozygous 1bp insertion (P648Tfs*2) that
172 disrupts *KMT2D* in the KDM5-inhibition sensitive SU-DHL-8 cells, generating three
173 clones where a single allele had been reverted to WT, two of which displayed increased
174 global H3K4me1 (K51 and K65; Supplementary Figure 4e). All of these clones were
175 more resistant to KDM5-inhibition with an average increase in AUC of 19% (Figure
176 2f), confirming that KDM5-inhibition sensitivity is altered by *KMT2D* mutations.

177

178 **KDM5-inhibition induces widespread increases in H3K4me3**

179 We hypothesised that increased H3K4me3 levels would drive a gene expression
180 programme responsible for the cytostatic and cytotoxic activity of KDM5-inhibition.
181 H3K4me3 ChIP-seq identified 11158 H3K4me3 peaks in untreated SU-DHL-6 cells
182 (Supplementary Table 2; Supplementary Figure 5a), with the majority (72.6%) located
183 at gene promoters (Figure 3a). KDM5-inhibition increased the average peak size
184 (Supplementary Figure 5b) and altered H3K4me3 levels at 2408 peaks, with 98%
185 demonstrating increased H3K4me3 (Supplementary Table 2; Figure 3b). Only a third

186 of these peaks overlapped with promoters (Figure 3a), suggesting that KDM5-
187 inhibition may alter H3K4me3 deposition at both enhancers and promoters. This was
188 confirmed by overlaying intergenic regions regulated by KDM5-inhibition with ChIP-
189 seq data from GC-lymphoma cell lines (ENCODE) and primary GC B-cells
190 (BLUEPRINT (22)), which showed that 84-95% overlapped with the enhancer-
191 associated H3K4me1 mark (Supplementary Figure 5c+d). These intergenic regions also
192 largely showed deposition of H3K4me3 and H3K27ac, indicating that the majority are
193 active enhancers.

194

195 We also noted that promoters significantly altered by KDM5-inhibition displayed basal
196 levels of H3K4me3 that were significantly lower than the average promoter in SU-
197 DHL-6 (Figure 3c). These promoters also displayed low levels of H3K4me3 in other
198 cell lines (e.g. OCI-LY-7) and instead had higher levels of H3K4me1 (Supplementary
199 Figure 5e+f). A low H3K4me3/H3K4me1 ratio has previously been described to mark
200 promoters that are poised to respond to cellular signalling (26,27), and it is probable
201 that the KDM5 family maintains a poised configuration at these promoters by
202 preventing high levels of H3K4me3 deposition.

203

204 **KDM5-inhibition converts H3K4me1 to H3K4me3 at promoters**

205 To understand how *KMT2D* mutations alter H3K4me1 and H3K4me3, and the
206 influence this has on the response to KDM5-inhibition, we focused on WSU-DLCL2
207 clone #22 (WSU#22^{-/+}), where we had engineered a heterozygous 1bp deletion
208 (P95Qfs*35) that is typical of the *KMT2D* mutations seen in GC-lymphomas (Figure
209 2e). We first examined global changes in H3K4me3/me1 by ChIP-seq, and observed
210 moderate changes in H3K4me1 (1333 altered peaks; 62.3% decreased) between

211 untreated WSU-DLCL2 and WSU#22^{-/+} cells, with H3K4me3 minimally affected (49
212 altered peaks) (Supplementary Figure 6a-c; Supplementary Table 2). The response to
213 KDM5-inhibition was more dramatic, with H3K4me3 deposition broadly increased
214 (>99% of sites) in WSU-DLCL2 and WSU#22^{-/+} cells (4604/3244 peaks) while there
215 was a predominant reduction (>80%) in H3K4me1 levels (2469/3130 peaks)
216 (Supplementary Figure 6a-c; Supplementary Table 2).

217

218 We identified 10,259 promoters that were marked by H3K4me3 but not significantly
219 altered by KDM5-inhibition in WSU-DLCL2 or WSU#22^{-/+} cells, and 1958 promoters
220 with significantly altered H3K4me3 following KDM5-inhibition. As before
221 (Supplementary Figure 5e+f), we found the majority of promoters to display a typical
222 high H3K4me3/H3K4me1 ratio whilst the significantly altered promoters showed an
223 inverse low H3K4me3/H3K4me1 ratio (Figure 3d; Supplementary Figure 6d). Across
224 all promoters KDM5-inhibition reduced H3K4me1 and increased H3K4me3 (Figure
225 3d+e), although the degree of change was more striking in the H3K4me1
226 high/H3K4me3 low group (Figure 3d) and suggests that KDM5-inhibition activates
227 promoters by converting H3K4me1 into H3K4me3.

228

229 **KDM5-inhibition induces moderate changes in gene expression**

230 Genes differentially expressed (DE; FDR <0.05, log₂FC > 1 or <-1) by KDM5-
231 inhibition were identified by RNA-seq analysis of two sensitive (SU-DHL-6 and OCI-
232 LY-18) and one insensitive cell line (HT) treated with 1μM KDM5-inh1 for 24h or 72h.
233 Overall, a greater number of DE genes were observed at 72h versus 24h in all the cell
234 lines tested (Figure 3f; Supplementary Table 3) with the impact on expression most
235 striking in the SU-DHL-6 cell line (147 and 545 DE genes). Modest changes in

236 expression occurred in the other sensitive cell line OCI-LY-18 (52 and 83 DE genes)
237 and the insensitive cell line HT (13 and 95 DE genes). In all conditions, with the
238 exception of HT 72h, the majority of DE genes were upregulated, whilst there was a
239 greater overlap between the two sensitive cell lines (Supplementary Figure 7a-c).

240

241 Focusing on SU-DHL-6 and comparing our KDM5-inhibition RNA- and ChIP-seq data
242 at 72h, we observed that promoter H3K4me3 correlated with gene expression ($r=0.28$)
243 to a greater extent than enhancer H3K4me3 levels ($r=0.04$; versus nearest gene)
244 (Supplementary Figure 7d). This was more pronounced when selectively examining
245 upregulated genes (0.44 vs 0.02) and indicates that KDM5-inhibition activates gene
246 expression through promoters rather than enhancers, whilst gene downregulation may
247 be an indirect consequence downstream of H3K4me3 deposition. Overall, these results
248 indicate that KDM5-inhibition has a relatively modest impact upon gene expression
249 despite inducing widespread increases in H3K4me3.

250

251 **KDM5-inhibition regulates KMT2D dependent and independent genes.**

252 We next compared RNA-seq profiles between WSU-DLCL2 and WSU#22^{-/+} cells and
253 identified 445 DE genes, while parallel KDM5-inhibition led to 309 and 339 changes
254 in gene expression, which included 141 common transcripts (Supplementary Figure
255 7e+f). In total, 897 genes were either DE between WSU-DLCL2 and WSU#22^{-/+} or
256 following KDM5-inhibition, which were divided into seven discrete groups using K-
257 mean clustering (Figure 3g; Supplementary Table 3).

258

259 The majority of genes (71%) were regulated by either KMT2D (e.g. Clusters One and
260 Two) or KDM5-inhibition alone (e.g. Cluster Three). We also identified two clusters

261 (Clusters Four and Five) where changes in gene expression accompanying the
262 P95Qfs*35 mutation were effectively reversed following KDM5-inhibition. Cluster
263 Four contained genes which were downregulated by *KMT2D* loss (mean log₂FC = -
264 0.87) but upregulated by KDM5-inhibition in both WT and mutant cells (mean log₂FC
265 = 0.92 vs 1.75), including the cell-cycle regulator *CDKN1A* and several BCR-signalling
266 regulators (*LCK*, *TRAF3IP3*, *PRKCB*, *FCGR2B*). An inverse-relationship was
267 observed in Cluster Five, where genes were upregulated by *KMT2D* loss (mean log₂FC
268 = 0.31) but downregulated by KDM5-inhibition in WSU-DLCL2 and WSU#22^{-/+} cells
269 (mean log₂FC = -1.0 vs -1.1) (Figure 3g), including the apoptotic-regulator *BCL2*.

270

271 We next analysed how levels of promoter H3K4 methylation may regulate gene
272 expression in these clusters. Clusters upregulated by KDM5-inhibition (Three, Four
273 and Six) exhibited low basal H3K4me₃/high H3K4me₁, whereas the remaining clusters
274 had a typical high H3K4me₃/H3K4me₁ ratio (Figure 3h, Supplementary Figure 7g).
275 Although KDM5-inhibition reduced H3K4me₁ and increased H3K4me₃ within all the
276 clusters, its effect was most notable upon Clusters Three and Four, where it altered the
277 H3K4me₃/H3K4me₁ ratio to the extent that levels of H3K4me₃ surpassed H3K4me₁
278 (Figure 3i+j, Supplementary Figure 7g). Cluster Five in contrast displayed minimal
279 changes in H3K4me₃, supporting our previous observation that KDM5-inhibition may
280 indirectly downregulate gene expression. Across all clusters however, *KMT2D* loss
281 induced minimal changes to promoter H3K4me₁/me₃ (Supplementary Figure 7g),
282 indicating that *KMT2D* mutations may not regulate gene expression through H3K4
283 methylation.

284

285 **KDM5-inhibition regulates *KMT2D* and CREBBP target genes**

286 To further test whether KDM5-inhibition regulates KMT2D target genes, we used Gene
287 Set Enrichment Analysis (GSEA) (28) to compare our two RNA-seq series with a
288 manually-curated database of lymphoma and B-cell signatures, including signatures
289 derived from patient cohorts, *in vitro* analyses and conditional mouse models of
290 KMT2D and CREBBP loss (9,10,29-31). All four datasets generated in two recent
291 lymphoma *KMT2D* studies (9,10) were significantly enriched in both series, as were 28
292 signatures associated with CREBBP (Figure 4a; Supplementary Figure 8a;
293 Supplementary Table 3+4) and the HDAC3i BRD3308 (Supplementary Figure 8b),
294 recently proposed as a targeted therapy to reverse the effects of CREBBP loss (30,31).
295 Moreover, these CREBBP/KMT2D signatures were also enriched in our SU-DHL-6
296 and WSU-DLCL2/WSU#22^{-/+} H3K4me3 ChIP-seq data (Supplementary Figure 8a+c;
297 Supplementary Table 4+5), whilst the 2408 regions regulated by KDM5-inhibition in
298 SU-DHL-6 significantly overlapped with binding of KMT2D and CREBBP, with 62%
299 of the regions bound by KMT2D, 53% by CREBBP and 45% by both (Figure 4b;
300 Supplementary Figure 8d). In contrast, we detected modest enrichment for signatures
301 associated with *EZH2* mutations and EZH2i (32,33), and limited overlap between
302 KDM5-inhibition regulated regions and EZH2/SUZ12 binding (34)(Supplementary
303 Figure 8a-d).

304

305 We next investigated the enrichment of a range of histone marks and epigenetic-
306 regulators in our previously defined gene clusters in WSU-DLC2/WSU#22^{-/+} (Figure
307 3g), including H3K27ac, H3K27me3, KMT2D and CREBBP, in GC-lymphoma cell
308 lines (ENCODE) and GC B-cells (BLUEPRINT (22)). In agreement with our earlier
309 observations linking CREBBP to KDM5 regulated genes (Figure 4a+b), Cluster Four
310 displayed levels of H3K27ac and CREBBP binding that were noticeably higher than

311 any other cluster, including Cluster Three which is regulated by KDM5-inhibition but
312 not KMT2D loss (Figure 4c). Levels of KMT2D binding conversely did not appear to
313 be predictive of KDM5-inhibition response (Figure 4c; Supplementary 8e). Since
314 recent publications indicate that the major consequences of KMT2D loss may occur
315 through altering EP300 and KDM6A recruitment (13,14), we propose that *KMT2D*
316 mutations sensitise cells to KDM5i by altering the recruitment of other epigenetic
317 enzymes (e.g. EP300/CREBBP), thereby repressing the expression of a subset of genes
318 with an atypical epigenetic profile and a high dependency for H3K27ac, which can be
319 reactivated through KDM5-inhibition converting H3K4me1 into H3K4me3.

320

321 **KDM5-inhibition upregulates regulators of BCR-signalling.**

322 Pathway analysis of the genes associated with altered H3K4me3 in SU-DHL-6 revealed
323 pathways highly relevant to lymphoma biology, with the most enriched terms including
324 “Hematologic cancer”, “Adaptive immune system” and several pathways related to
325 BCR-signalling, whilst pathways related to GPCR signalling were predominantly
326 enriched in our H3K4me3 analysis of KDM5-inh1 treated WSU-DLCL2/WSU#22
327 cells (Supplementary Figure 8a+f; Supplementary Table 5). Similarly, GSEA (28) of
328 our RNA-seq data identified the pathway “Adaptive immune system” as being strongly
329 enriched across all conditions, whilst pathways related to GPCR-signalling were
330 strongly enriched in SU-DHL-6, OCI-LY-18 and WSU-DLCL2/WSU#22^{-/+} cells
331 (Figure 4d+e; Supplementary Table 4), indicating that KDM5-inhibition may regulate
332 B-cell signalling. This was further supported by our observation that KDM5-inhibition
333 primarily targets genes with high levels of promoter H3K4me1 (Supplementary Figure
334 5e-f), which has been described as a signature of signal-responsive genes (26,27),

335 whilst BCR-signalling regulators were identified within the KDM5-inhibition and
336 KMT2D regulated genes in Cluster Four (Figure 3g-j).

337

338 Amongst the negative-regulators of BCR-signalling induced by KDM5-inh1 was the
339 tyrosine phosphatase SHP-1 (*PTPN6*; Figure 4f) (35,36), which is regulated by
340 KMT2D (9) and CREBBP (29), and subject to low-frequency mutations and silencing
341 in lymphoma (37), alongside a range of receptors able to recruit and activate SHP-1
342 including *FCGR2B*, *FCRL3/5*, *CD72* and *LAIR1* (Figure 4g). KDM5-inhibition
343 increased H3K4me3 and reduced H3K4me1 levels across the *PTPN6* promoter in SU-
344 DHL-6 cells, without altering H3K27ac, and upregulated SHP-1 expression (Figure 5a;
345 Supplementary Figure 9a+b). Increased promoter H3K4me3 levels were observed for
346 *PTPN6* and other BCR-signalling regulators in primary FL cell-suspensions following
347 KDM5-inhibition (Supplementary Figure 9c), while these BCR-signalling regulators
348 were also induced by Compound-48 and KDM5-C70 in SU-DHL-6 cells
349 (Supplementary Figure 9d), indicating that these genes are specifically regulated by the
350 demethylase activity of the KDM5 family.

351

352 **KDM5-inhibition results in a more rapid curtailment of BCR-signalling**

353 To determine whether the increased expression of negative-regulators such as SHP-1
354 (35,36) altered BCR-signalling, the phosphorylation of SYK, a proximal kinase
355 activated following BCR engagement, was examined in the IgM⁺ SU-DHL-6 and OCI-
356 LY-18 cells (Supplementary Figure 10a) pre-treated with DMSO or KDM5-inh1 for
357 72h and then stimulated with anti-IgM F(ab')₂. KDM5-inh1 pre-treatment reduced
358 levels of SYK phosphorylation at later time points (1-4h) following sIgM engagement,
359 whilst the initial induction of SYK phosphorylation at 10 minutes was unaffected by

360 KDM5-inhibition (Figure 5b, Supplementary Figure 10b+c). Effects on sIgM were
361 selective since KDM5-inhibition did not affect surface expression of sIgM
362 (Supplementary Figure 10a) or intracellular calcium release (Supplementary Figure
363 10d+e). By contrast, we observed KDM5-inhibition to have no impact upon SYK
364 phosphorylation in the KDM5-inhibition insensitive anti-IgM responsive OCI-LY-7
365 cells (Figure 5b; Supplementary Figure 10b+c) and the KDM5-inhibition insensitive
366 HT cells, which had extremely high constitutive levels of BCR-signalling and were
367 unresponsive to anti-IgM stimulation (data not shown) (38). The kinetics of signalling
368 without alterations of sIgM expression suggested a more rapid curtailment in BCR-
369 signalling in KDM5-inhibition sensitive cells, consistent with the expected
370 consequence of increasing the expression of regulators such as SHP-1 (39).

371

372 **KDM5-inhibition modulates the expression of BCL2 family members**

373 Amongst the downregulated genes, we observed reduced expression of the anti-
374 apoptotic BCL2. All three KDM5i tested consistently reduced BCL2 protein expression
375 in t(14;18) positive cell lines (Figure 5c; Supplementary Figure 11a), although
376 sensitivity to KDM5-inhibition and the BCL2i Venetoclax varied ($r=0.38$, $p=0.31$),
377 indicating that response to KDM5-inhibition is not solely dependent on BCL2
378 (Supplementary Figure 11b+c). The mechanism of BCL2 downregulation appeared to
379 be an indirect effect of KDM5-inhibition, as we observed no clear changes in
380 H3K4me3/me1 or H3K27ac across the *BCL2* promoter (Supplementary Figure 9a) or
381 at enhancers contained within *BCL2* or the IGH locus (data not shown), consistent with
382 earlier observations that downregulated genes do not correlate with H3K4me3
383 deposition (Supplementary Figure 7d+g).

384

385 We next analysed the expression of BCL2 alongside other family members in SU-DHL-
386 6 and HT cells treated with KDM5-inh1 for two and five days (OCI-LY-18 cells were
387 not examined due to high levels of drug-induced cell death). Minimal changes were
388 observed in the insensitive HT cells, however decreased BCL2 and BCL-XL
389 expression, alongside increasing expression of the pro-apoptotic NOXA, BIM_L and
390 BIM_{EL}, were observed at day five in SU-DHL-6 (Figure 5d+e). These changes preceded
391 the onset of apoptosis at day two (Supplementary Figure 11d+e), whilst KDM5-
392 inhibition also reduced *BCL2* and *BCL-XL* mRNA expression in primary FL cell-
393 suspensions (Supplementary Figure 9c). Overall, these data indicate that KDM5-
394 inhibition shifts the balance of BCL2 family members towards a pro-apoptotic response
395 in sensitive cells.

396

397 **KDM5-inhibition synergises with MCL1 and BTK inhibitors**

398 Given the ability of KDM5-inhibition to regulate BCR-signalling and BCL2 family
399 members, we next tested whether KDM5-inhibition could synergise with the BH3
400 mimetics Venetoclax (BCL2i) (40) and S63845 (MCL1i) (41) and the BTKi Ibrutinib
401 (42), which are all under clinical-investigation for GC-lymphomas. Although we were
402 unable to detect synergy in SU-DHL-6 cells due to their high response to KDM5-
403 inhibition alone, we observed KDM5-inh1 to highly synergise with S63845 in
404 KARPAS-422 (*KMT2D*^{-/+}) and with Ibrutinib in WSU-DLCL2 (*KMT2D*^{+/+}) cells
405 (Figure 5f+g; Supplementary Figure 12, Supplementary Table 7). The synergy with the
406 MCL1i S63845 is likely explained by KDM5-inhibition downregulating the expression
407 of the two other major negative regulators of apoptosis, BCL2 and BCL-XL, whilst the
408 synergy with ibrutinib could be due to altered expression of BCR-signalling regulators
409 and/or BCL2 family members.

410

411 **Loss of *KDM5A* alone does not alter proliferation or survival**

412 We next used CRISPR to examine how *KDM5A* and *KDM5C* regulate previously
413 identified *KDM5*-inhibition target genes and determine whether any *KDM5* isoform
414 alone is essential for lymphoma survival. *KDM5A* and *KDM5C* knockout clones were
415 successfully isolated from *KMT2D* WT WSU-DLCL2 cells (Supplementary Figure
416 13a) however we were only able to generate *KDM5A* knockout clones from *KMT2D*
417 mutant SU-DHL-6 cells (Figure 6a). Loss of *KDM5A/KDM5C* in WSU-DLCL2 or
418 *KDM5A* in SU-DHL-6 cells had minimal impact on H3K4me3 levels (Figure 6a;
419 Supplementary Figure 13a) or upon cell proliferation or survival (data not shown).
420 *KDM5A* knockout did upregulate the expression of several *KDM5* target genes in SU-
421 DHL-6 (e.g. *FCRL5*, *DUSP6*), although to a lesser extent than *KDM5*-inhibition
422 (Figure 6b).

423

424 We next analysed whether the anti-proliferative response to *KDM5*-inhibition was
425 altered in *KDM5A/KDM5C* knockout cells, reasoning that it would be blunted if
426 *KDM5*-inhibition primarily functioned through either isoform alone, and found instead
427 that silencing of *KDM5A* and *KDM5C* both increased sensitivity to *KDM5*-inhibition
428 in SU-DHL-6 and WSU-DLCL2 (Figure 6c; Supplementary Figure 13b). Whilst it is
429 possible that losing or inhibiting *KDM5C* alone may be lethal in *KMT2D* mutant cells,
430 we believe it is more likely that multiple isoforms must be inhibited to robustly induce
431 gene expression and an anti-proliferative response, which is supported by previous
432 reports of redundancy in the *KDM5* (43,44) and other *KDM* families (45,46), global
433 H3K4me3 levels remaining stable in our single isoform knockout models and *KDM5A*
434 knockout only partially activating *KDM5*-inhibition regulated genes.

435

436 **KDM5-inh1 has *in vivo* activity against *KMT2D* mutant xenografts**

437 In order to test the *in vivo* efficacy of KDM5-inh1, *KMT2D* mutant SU-DHL-6 cells
438 were xenografted subcutaneously into NOD/SCID mice. Mice were orally administered
439 vehicle, 50mg/kg KDM5-inh1 daily or 10mg/kg Ibrutinib (positive control) for 21 days,
440 with a dosing-holiday scheduled between days 8-14 for the KDM5-inh1 group after
441 preliminary experiments indicated that this regime would be efficacious and tolerable.
442 KDM5-inh1 was well tolerated throughout the study, with weight loss <20% and no
443 other signs of toxicity observed (Supplementary Figure 14a-c). Levels of H3K4me3
444 were variable at the study endpoint, although increased H3K4me3 and reduced BCL2
445 expression were observed in the tumours of mice treated with KDM5-inh1 for seven
446 days (Figure 6d; Supplementary Figure 14d). After seven days of treatment, tumour
447 growth inhibition (TGI) of 65% was observed for the KDM5-inh1 group, and while the
448 tumours partially recovered during the dosing-holiday, TGI values of 54-66% were
449 maintained until day 17 when the vehicle group was sacrificed (Figure 6e).

450

451

452 **Discussion**

453

454 The *KMT2* methyltransferases are one of the most highly disrupted gene families across
455 cancer (11), most notably within the GC-lymphomas where 80% of FL (1-4) and 30%
456 of GCB-DLBCL cases harbour *KMT2D* mutations (5-7), alongside mutations in other
457 epigenetic-regulatory genes including *CREBBP* (29,30,47-49) and *EZH2* (50-52). The
458 potential of precisely targeting these mutations has recently been established by the
459 development of EZH2i, with these compounds partially selective towards *EZH2* mutant
460 FL patients in phase II clinical trials (33,53,54). The observation that *CREBBP* mutant
461 lymphomas are HDAC3-dependent has also presented another potential therapeutic
462 target (30,31), and hints that pharmacological inhibition of antagonistic enzymes may
463 be an effective strategy for targeting loss-of-function epigenetic mutations. Despite the
464 high frequency of *KMT2D* mutations in GC-lymphomas and other malignancies, no
465 means of therapeutically targeting these lesions has been reported. We therefore
466 examined whether inhibiting the KDM5 family could ameliorate the loss of *KMT2D* by
467 stabilising H3K4 methylation and restoring the expression of genes normally regulated
468 by *KMT2D*.

469

470 KDM5-inhibition increased global levels of the promoter-associated H3K4me3 and
471 induced significant cytostatic and cytotoxic responses in *KMT2D* mutant cell lines *in*
472 *vitro* and tumour growth inhibition *in vivo*. In this report we describe two mechanisms
473 through which KDM5i function. Firstly, we observed increased expression of negative-
474 regulators of B-cell signalling, including *PTPN6*, resulting in the more rapid
475 curtailment of BCR-signalling in cells treated with KDM5i. Secondly, KDM5-
476 inhibition induced striking reductions in *BCL2* expression in t(14;18) positive cell lines
477 alongside altering the expression of other *BCL2* family members. Although

478 pharmacologically targeting BCL2 alone appears to have modest single-agent activity
479 in GC-lymphomas (55,56), the simultaneous modulation of pro- and anti-apoptotic
480 regulators, alongside the loss of survival signals from the BCR, seems likely to drive
481 the induction of apoptosis triggered by KDM5-inhibition. Encouragingly, our data
482 indicate that KDM5i are able to synergise with therapeutics agents targeting these
483 pathways, although further *in vivo* studies are required to establish the therapeutic
484 window of KDM5-inhibition, both alone and in combination, and whether it impacts
485 upon normal B-cell functions. Our data is also consistent with prior reports of
486 significant redundancy within the KDM5 (43,44), and other KDM families (45,46), and
487 indicates that inhibition of multiple KDM5 members may be required to achieve a
488 therapeutic response, which should be considered in the further development of
489 KDM5i.

490

491 KDM5-inhibition sensitivity was confirmed to be highly dependent on *KMT2D* by
492 generating and correcting *KMT2D* mutations in WT and mutant cell lines respectively,
493 with alteration of a single allele capable of shifting the response to KDM5-inhibition.
494 Our epigenetic and transcriptomic analyses revealed that KDM5-inhibition activates
495 both KMT2D-dependent and -independent gene networks, and in particular targets
496 promoters marked by high levels of H3K4me1. High H3K4me1 levels may act to
497 maintain these promoters in a poised configuration, and have previously been described
498 to mark the promoters of stimuli-responsive genes with roles in signal transduction
499 (26,27). This is consistent with our observation of KDM5-inhibition increasing the
500 expression of BCR-signalling regulators, while *KMT2D* mutations have been shown to
501 alter B-cell signalling by preventing the upregulation of negative-regulators following
502 CD40-stimulation (10).

503

504 Despite the evidence presented here that KDM5i can reactivate KMT2D target genes,
505 by increasing H3K4me3 at the expense of H3K4me1, KDM5-inhibition does not
506 directly reverse the epigenetic consequences of losing the mono-methyltransferase
507 activity of KMT2D. Indeed inhibition of LSD1, the direct antagonist of the
508 methyltransferase activity of KMT2D, has previously been shown to be ineffective in
509 lymphoma, suggesting that restoring H3K4me1 alone is not sufficient to restore
510 KMT2D-regulated genes (57). One potential explanation worth considering is the ability
511 of KMT2D to recruit the H3K27 acetyltransferases EP300/CREBBP and demethylase
512 KDM6A (13,14), which would imply that loss of H3K4me1 is only one part of a wider
513 epigenetic disruption induced by *KMT2D* mutations.

514

515 Our data indicate that KMT2D-dependant genes upregulated by KDM5-inhibition
516 (Cluster Four) display strikingly high levels of H3K27ac and CREBBP-binding in
517 addition to a low H3K4me3/H3K4me1 ratio. Further studies are required to establish
518 whether mutations in *KMT2D* alter the recruitment of EP300/CREBBP to these
519 promoters, and while the extent to which epigenetic mutations overlap in lymphoma is
520 a key outstanding question, our data indicates that this subset of genes is likely to be
521 disrupted by multiple mutations. Systematically identifying genes regulated by multiple
522 epigenetic-mutations may be one way to distil their key targets and determine the most
523 effective therapeutic-agents and combinations to target these lesions.

524

525 In summary, this report establishes the potential of KDM5-inhibition as a targeted
526 therapy for GC-lymphomas that is able to reactivate the expression of genes normally
527 regulated by KMT2D. In particular, the increased expression of negative-regulators of

528 B-cell signalling results in a curtailment of pro-survival signals and decreases the
529 expression of BCL2 and other BCL2 family proteins. Notably, the response to KDM5-
530 inhibition appears to be highly dependent on the presence of *KMT2D* mutations and
531 raises the question as to whether KDM5i may be effective in other malignancies
532 harbouring *KMT2D* lesions, or indeed mutations in other *KMT2* methyltransferases.

533

534 **Acknowledgements**

535 We would like to thank EpiTherapeutics and Gilead for providing us with KDM5-inh1
536 and general advice throughout the project, in particular Lars-Ole Gerlach, Kristian
537 Helin, Daniela Kleine-Kohlbrecher and Peter Staller (EpiTherapeutics).

538

539 **Authorship contributions**

540 J.F. and J.H. conceived the study; J.H., G.P. A.M. and J.F. designed the study; J.H.,
541 A.D., G.P. and J.F. wrote the manuscript; J.G., P.J., J.O., S.I. and A.C. identified,
542 contributed and prepared patient samples for the project; J.H., F.B.C and J.W.
543 performed bioinformatic analysis; J.H., L.K., A.D., A.Y., T.R., A.F.A., S.A., K.C.,
544 M.P., J.D., D.B., K.K. and E.K. performed experiments; J.H., L.K., A.D., A.Y. and J.F.
545 analysed the data; R.N., U.O. and A.M. contributed reagents and interpretation of data;
546 All authors read, critically reviewed and approved the manuscript.

547 **Methods**

548 **Cell culture**

549 All cell lines were cultured in a 37°C, 5% CO₂ humidified incubator using RPMI-1640
550 supplemented with 10% FBS, 1% L-glutamine and 1% Pen-Strep, except OCI-LY-1
551 and OCI-LY-7, which were cultured in IMDM with 20% FBS, 1% L-glutamine and 1%
552 Pen-Strep (Supplementary Table 8). Cell lines were acquired from DSMZ or an
553 institute tissue-bank. Identity was confirmed by STR sequencing and regularly checked
554 by Sanger sequencing of unique mutations and for Mycoplasma contamination.

555

556 Primary FL cell-suspensions were defrosted at 37°C and layered onto 3ml of
557 lymphoprep (STEMcell Technologies). Lymphocytes were isolated by centrifugation
558 at 1150g for 12 minutes, washed in RPMI and resuspended in fresh RPMI before
559 treatment. Written consent was obtained for the collection and use of specimens for
560 research purposes with ethical approval obtained from the London Research Ethics
561 Committee of the East London and the City Health authority (10/H0704/65,
562 06/Q0605/69) and Southampton and South West Hampshire (t228/02/t).

563

564 **Western blots**

565 To assess histone mark levels, an isotonic lysis buffer (20mM Tris, 100mM NaCl, 5mM
566 MgCl₂, 10% glycerol, 0.2% NP40, 0.5mM DTT) and centrifugation was used to isolate
567 nuclei, which were lysed in a high-salt buffer (50mM Tris, 600mM NaCl, 10%
568 glycerol, 0.2% NP40, 0.5mM DTT) followed by sonication to fragment chromatin
569 (Diagenode Bioruptor). Buffers were supplemented with phosphatase and Complete
570 ULTRA protease inhibitor cocktails (Roche) and lysates quantified by Pierce 660nm
571 Protein Assay Reagent (ThermoFisher). 1-2.5µg of nuclear protein was loaded in 4-

572 12% Bis-Tris gels (NuPAGE), resolved by SDS-PAGE and transferred to
573 polyvinylidene fluoride membranes via the iBlot™ transfer device (Invitrogen). After
574 blocking with 5% BSA/Milk in Tris-buffered saline, membranes were probed with
575 primary antibody, stained with horseradish peroxidase-conjugated secondary
576 antibodies (DAKO) and bands detected using ECL Plus (GE Healthcare) or
577 SuperSignal West Femto (ThermoFisher). To examine multiple histone marks, equal
578 amounts of protein were loaded onto multiple gels from a single loading solution, and
579 quantified relative to H3.

580

581 For total protein analysis, western blots were performed as before except that cells were
582 lysed in RIPA buffer (150mM NaCl, 1% NP-40, 0.5% sodium deoxycholate, 0.1%
583 sodium-dodecyl-sulphate, 50mM tris(hydroxymethyl)aminomethane hydrochloride,
584 pH 8.0), supplemented with 1X protease inhibitor and phosphatase inhibitor cocktail 2
585 and 3 (Sigma-Aldrich), for 30 minutes. Densitometry analysis was performed using
586 ImageJ software and all the antibodies used are listed in Supplementary Table 9

587

588 **Proliferation and apoptosis assays**

589 2000 cells were seeded in 100µl growth media in triplicate in 96-well plates 24h before
590 treatment, followed by treatment with DMSO and 6 concentrations of KDM5i diluted
591 8-fold (0.0003-10µM) in 100µl of growth medium. The plates were incubated for five
592 days, when viable cell numbers were determined using the Guava ViaCount assay
593 (Millipore) or CellTitreGlo (Promega). The percentage of apoptotic cells was
594 quantified by the Guava Nexin assay (Millipore), which measures binding of Annexin
595 V to phosphatidyl serines and the incorporation of 7-AAD, a cell impermeable dye.

596 Apoptotic cells were defined as Annexin V⁺/7-AAD⁺, early-apoptotic as Annexin
597 V⁺/7-AAD⁻ and nucleated debris as Annexin V⁻/7-AAD⁺.

598

599 For 10-day treatments, 20,000 cells were seeded in 1ml in 12-well plates and incubated
600 overnight. The cells were then treated with DMSO or KDM5-inh1 (0.0024-10 μ M) and
601 incubated for 5 days. Viable cell numbers were determined, and the cells re-seeded in
602 triplicate in 96-well plates at 4000 cells/well and treated with the same concentration
603 of KDM5-inh1 or DMSO as before. Viable cell numbers were determined by Guava
604 ViaCount assay after a further 5-day incubation.

605

606 **Cell-cycle analysis**

607 After treatment with DMSO or KDM5-inh1 for 72h, cells were permeabilized in ice-
608 cold 70% ethanol, stored at -80°C and stained in PBS containing 50 μ g/ml propidium
609 iodide and 100 μ g/ml RNase A. DNA content was then quantified using the YG610/20
610 filter on a Fortessa II flow cytometer.

611

612 **Surface IgM analysis**

613 Cells were washed, re-suspended in FACS buffer (1% BSA, 4mM
614 ethylenediaminetetraacetic acid (EDTA) and 0.15mM NaN₃ in PBS) and stained for
615 surface IgM expression (5x10⁵ cells/100 μ l) in the dark on ice for 30 minutes, using R-
616 Phycoerythrin-conjugated anti-IgM (DAKO). Following incubation, cells were
617 washed, re-suspended in FACS buffer and 1x10⁴ lymphocytes were acquired on a
618 FACS Canto (BD Biosciences). Analysis of mean fluorescence intensities was
619 performed with FlowJo software.

620

621 **Synergy analysis**

622 Cells were treated with 5 concentrations of KDM5-inh1 for 5 days as per the standard
623 proliferation assay described above, except that cells were also treated with 5
624 concentrations of S63845 and Venetoclax for 2 days or Ibrutinib for 3 days. Synergy
625 was assessed for each combination using the DrugComb portal
626 (<https://drugcomb.fimm.fi/analysis/>).

627

628 **RNA extraction**

629 RNA was extracted using QIAGEN RNeasy kits including an on-column DNase step.
630 RNA for sequencing was determined to be of high-quality by Agilent Bioanalyser or
631 Tapestation (RIN > 9.5).

632

633 **cDNA synthesis and qRT-PCR**

634 cDNA was synthesised using the high capacity cDNA reverse transcription kit
635 (ThermoFisher) and qPCR performed using the SsoAdvanced™ Universal
636 SYBR® Green Supermix (BioRad). Reactions were performed in triplicate and
637 normalised to GAPDH. All primer sequences are listed in Supplementary Table 10.

638

639 **ChIP-PCR and –seq**

640 ChIP reactions were prepared using a modified version of the Active Motif ChIP-IT
641 High Sensitivity Kit. For cell lines, 5-15 million cells were treated for 72h with DMSO
642 or 1µM KDM5-inh1, cross-linked in a 1% formaldehyde/PBS solution for 5 minutes,
643 washed in PBS, and nuclei isolated by 5 minute incubation on ice in a cytoplasmic lysis
644 buffer (50mM Tris·Cl, 140mM NaCl, 1.5mM MgCl₂, 0.5% (v/v) Nonidet P-40
645 (1.06g/ml)) and centrifugation. Nuclei were sonicated using a BioRuptor for 10-20

646 cycles of 30s on (high)/60s off. After confirming correct fragmentation of input DNA,
647 ChIP reactions were performed overnight at 4°C (antibodies listed in Supplementary
648 Table 9), followed by DNA precipitation with agarose beads, reversal of cross-links
649 and purification of DNA by columns. Samples were analyzed by qPCR using the probes
650 listed in Supplementary Table 10. Lymphocytes from primary FL cell-suspensions
651 were examined identically except that 1-5 million cells were used per ChIP and that the
652 cells were treated for 48h. For ChIP-seq, the chromatin was spiked with 15ng of
653 *Drosophila* chromatin (Active Motif; 53083) and ChIP was performed with an anti-
654 *Drosophila* chromatin antibody (Active Motif; 61686) alongside the
655 H3K4me3/H3K4me1 antibodies.

656 Libraries were prepared for sequencing using the NEBNext Ultra II and Multiplex
657 Oligios for Illumina kits (New England Biolabs) according to the manufacturers
658 protocol. Briefly, ChIP and input DNA were end-repaired, adaptors ligated and size-
659 selected using SPRIselect beads for 300-400bp DNA fragments and amplified by PCR.
660 Correct library size (400-500bp) was confirmed by TapeStation. Sequencing was
661 performed on the Illumina HiSeq 4000 to generate 75bp paired-end reads or NextSeq
662 500 to generate 40bp single-ended reads.

663

664 **CRISPR**

665 To generate *KMT2D* mutant cells, four pooled guide-RNAs (gRNAs) were designed
666 targeting exon 3 of *KMT2D*, whilst individual gRNAs were used for KDM5A/KDM5C
667 (Supplementary Table 11). gRNAs were combined with tracrRNA at equimolar
668 concentrations, heated at 95°C before cooling to anneal. 460pmol of the
669 gRNA/tracrRNA pool was then complexed with 401pmol of Cas9 protein (Alt-R Cas9

670 Nuclease 3NLS; IDT) and transfected by Nucleofection (Supplementary Table 12).
671 After transfection, cells were left to recover in 4ml of complete growth medium and
672 after 48h a cell-sorter was used to isolate single cell clones. Editing was identified by
673 Sanger sequencing and validated by TA-cloning for complex mutations
674 (Supplementary Table 1). To correct the 1bp insertion present in *KMT2D* within SU-
675 DHL-8 cells, CRISPR was performed as above except that a donor-template containing
676 119bp of WT sequence, with a silent mutation to alter the PAM site, was co-transfected
677 alongside the gRNA (targeting the mutation site) and Cas9 protein.

678

679 **Xenograft studies**

680 SU-DHL-6 xenograft studies were performed by Crown Bioscience Inc. (Beijing). 24h
681 after irradiation with Co^{60} (150 rads), 5×10^6 SU-DHL-6 cells (in 0.1ml PBS mixed with
682 matrigel 1:1) were inoculated subcutaneously into the right flank of NOD/SCID mice
683 (weighing 18-20g). Once tumours reached an average size of $100mm^3$, mice were
684 randomized into three groups of 10; vehicle (6% Captisol + 94% ddWater, pH=2),
685 KDM5-inh1 and ibrutinib. Mice were orally dosed daily with 50mg/kg KDM5-inh1
686 and 10mg/kg ibrutinib up to 21 days, with a scheduled dosing holiday for the KDM5-
687 inh1 group between days 8-14. Six mice were additionally randomized into two groups
688 (n=3) and treated with vehicle or 50mg/kg KDM5-inh1 for 1 week. Tumour volumes
689 were calculated in two dimensions 3x a week. Mice were euthanized when the mean
690 tumour size of the vehicle group exceeded $2000mm^3$ or once the study endpoint was
691 reached.

692 **References**

- 693 1. Okosun J, Bödör C, Wang J, Araf S, Yang C-Y, Pan C, et al. Integrated genomic
694 analysis identifies recurrent mutations and evolution patterns driving the
695 initiation and progression of follicular lymphoma. *Nat Genet.* Nature Publishing
696 Group; 2014;46:176–81.
- 697 2. Pasqualucci L, Khiabani H, Fangazio M, Vasishtha M, Messina M, Holmes
698 AB, et al. Genetics of follicular lymphoma transformation. *Cell Rep.* Elsevier;
699 2014;6:130–40.
- 700 3. Green MR, Kihira S, Liu CL, Nair RV, Salari R, Gentles AJ, et al. Mutations in
701 early follicular lymphoma progenitors are associated with suppressed antigen
702 presentation. *Proceedings of the National Academy of Sciences.* National Acad
703 Sciences; 2015;112:E1116–25.
- 704 4. Araf S, Okosun J, Koniali L, Fitzgibbon J, Heward J. Epigenetic dysregulation in
705 follicular lymphoma. *Epigenomics.* 2016;8:77–84.
- 706 5. Chapuy B, Stewart C, Dunford AJ, Kim J, Kamburov A, Redd RA, et al.
707 Molecular subtypes of diffuse large B cell lymphoma are associated with distinct
708 pathogenic mechanisms and outcomes. *Nature medicine.* Nature Publishing
709 Group; 2018;15:1.
- 710 6. Schmitz R, Wright GW, Huang DW, Johnson CA, Phelan JD, Wang JQ, et al.
711 Genetics and Pathogenesis of Diffuse Large B-Cell Lymphoma. *N Engl J Med.*
712 2018;378:1396–407.
- 713 7. Reddy A, Zhang J, Davis NS, Moffitt AB, Love CL, Waldrop A, et al. Genetic
714 and Functional Drivers of Diffuse Large B Cell Lymphoma. *Cell.* Elsevier;
715 2017;171:481–494.e15.
- 716 8. Morin RD, Mendez-Lago M, Mungall AJ, Goya R, Mungall KL, Corbett RD, et
717 al. Frequent mutation of histone-modifying genes in non-Hodgkin lymphoma.
718 *Nature.* Nature Publishing Group; 2011;476:298–303.
- 719 9. Zhang J, Dominguez-Sola D, Hussein S, Lee J-E, Holmes AB, Bansal M, et al.
720 Disruption of KMT2D perturbs germinal center B cell development and
721 promotes lymphomagenesis. *Nature medicine.* Nature Publishing Group;
722 2015;21:1190–8.
- 723 10. Ortega-Molina A, Boss IW, Canela A, Pan H, Jiang Y, Zhao C, et al. The histone
724 lysine methyltransferase KMT2D sustains a gene expression program that
725 represses B cell lymphoma development. *Nature medicine.* Nature Publishing
726 Group; 2015;21:1199–208.
- 727 11. Rao RC, Dou Y. Hijacked in cancer: the KMT2 (MLL) family of
728 methyltransferases. *Nat Rev Cancer.* Nature Publishing Group; 2015;15:334.
- 729 12. Shlyueva D, Stampfel G, Stark A. Transcriptional enhancers: from properties to
730 genome-wide predictions. *Nature reviews Genetics.* Nature Publishing Group;
731 2014;15:272–86.
- 732 13. Dorigi KM, Swigut T, Henriques T, Bhanu NV, Scruggs BS, Nady N, et al.
733 Mll3 and Mll4 Facilitate Enhancer RNA Synthesis and Transcription from

- 734 Promoters Independently of H3K4 Monomethylation. *Molecular cell*. Elsevier;
735 2017;66:568–576.e4.
- 736 14. Wang S-P, Tang Z, Chen C-W, Shimada M, Koche RP, Wang L-H, et al. A
737 UTX-MLL4-p300 Transcriptional Regulatory Network Coordinately Shapes
738 Active Enhancer Landscapes for Eliciting Transcription. *Molecular cell*.
739 Elsevier; 2017;67:308–321.e6.
- 740 15. Lindsley AW, Saal HM, Burrow TA, Hopkin RJ, Shchelochkov O, Khandelwal
741 P, et al. Defects of B-cell terminal differentiation in patients with type-1 Kabuki
742 syndrome. *Journal of Allergy and Clinical Immunology*. Mosby; 2016;137:179–
743 187.e10.
- 744 16. Ng SB, Bigham AW, Buckingham KJ, Hannibal MC, McMillin MJ, Gildersleeve
745 HI, et al. Exome sequencing identifies MLL2 mutations as a cause of Kabuki
746 syndrome. *Nat Genet*. Nature Publishing Group; 2010;42:790–3.
- 747 17. Rasmussen PB, Staller P. The KDM5 family of histone demethylases as targets
748 in oncology drug discovery. *Epigenomics*. 2014;6:277–86.
- 749 18. Sharma SV, Lee DY, Li B, Quinlan MP, Takahashi F, Maheswaran S, et al. A
750 chromatin-mediated reversible drug-tolerant state in cancer cell subpopulations.
751 *Cell*. Elsevier; 2010;141:69–80.
- 752 19. Facompre ND, Harmeyer KM, Sole X, Kabraji S, Belden Z, Sahu V, et al.
753 JARID1B Enables Transit between Distinct States of the Stem-like Cell
754 Population in Oral Cancers. *Cancer research*. American Association for Cancer
755 Research; 2016;76:5538–49.
- 756 20. Roesch A, Vultur A, Bogeski I, Wang H, Zimmermann KM, Speicher D, et al.
757 Overcoming intrinsic multidrug resistance in melanoma by blocking the
758 mitochondrial respiratory chain of slow-cycling JARID1B(high) cells. *Cancer*
759 *Cell*. Elsevier; 2013;23:811–25.
- 760 21. Richter J, Schlesner M, Hoffmann S, Kreuz M, Leich E, Burkhardt B, et al.
761 Recurrent mutation of the ID3 gene in Burkitt lymphoma identified by integrated
762 genome, exome and transcriptome sequencing. *Nat Genet*. Nature Publishing
763 Group; 2012;44:1316–20.
- 764 22. Stunnenberg HG, International Human Epigenome Consortium, Hirst M. The
765 International Human Epigenome Consortium: A Blueprint for Scientific
766 Collaboration and Discovery. *Cell*. Elsevier; 2016;167:1145–9.
- 767 23. Paroni G, Bolis M, Zanetti A, Ubezio P, Helin K, Staller P, et al. HER2-positive
768 breast-cancer cell lines are sensitive to KDM5 inhibition: definition of a gene-
769 expression model for the selection of sensitive cases. *Oncogene*. Nature
770 Publishing Group; 2018;12:1–2689.
- 771 24. Liang J, Zhang B, Labadie S, Ortwine DF, Vinogradova M, Kiefer JR, et al.
772 Lead optimization of a pyrazolo[1,5-a]pyrimidin-7(4H)-one scaffold to identify
773 potent, selective and orally bioavailable KDM5 inhibitors suitable for in vivo
774 biological studies. *Bioorganic & medicinal chemistry letters*. Pergamon;
775 2016;26:4036–41.

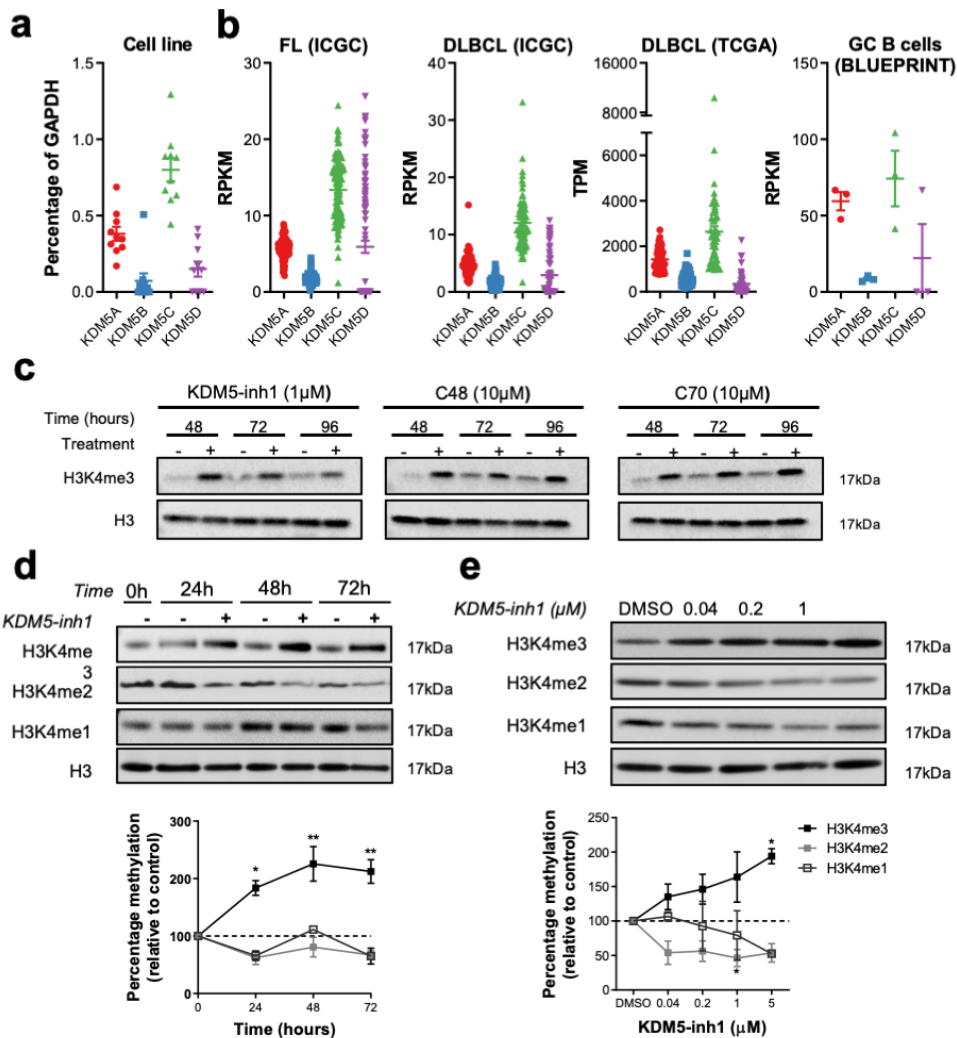
- 776 25. Johansson C, Velupillai S, Tumber A, Szykowska A, Hookway ES, Nowak RP,
777 et al. Structural analysis of human KDM5B guides histone demethylase inhibitor
778 development. *Nat Chem Biol.* Nature Publishing Group; 2016;12:539–45.
- 779 26. Cheng J, Blum R, Bowman C, Hu D, Shilatifard A, Shen S, et al. A role for
780 H3K4 monomethylation in gene repression and partitioning of chromatin
781 readers. *Molecular cell.* Elsevier; 2014;53:979–92.
- 782 27. Scruggs BS, Gilchrist DA, Nechaev S, Muse GW, Burkholder A, Fargo DC, et
783 al. Bidirectional Transcription Arises from Two Distinct Hubs of Transcription
784 Factor Binding and Active Chromatin. *Molecular cell.* Elsevier; 2015;58:1101–
785 12.
- 786 28. Subramanian A, Tamayo P, Mootha VK, Mukherjee S, Ebert BL, Gillette MA, et
787 al. Gene set enrichment analysis: A knowledge-based approach for interpreting
788 genome-wide expression profiles. *Proceedings of the National Academy of
789 Sciences of the United States of America.* National Academy of Sciences;
790 2005;102:15545–50.
- 791 29. Zhang J, Vlasevska S, Wells VA, Nataraj S, Holmes AB, Duval R, et al. The
792 CREBBP Acetyltransferase Is a Haploinsufficient Tumor Suppressor in B-cell
793 Lymphoma. *Cancer Discov.* American Association for Cancer Research;
794 2017;7:322–37.
- 795 30. Jiang Y, Ortega-Molina A, Geng H, Ying H-Y, Hatzi K, Parsa S, et al. CREBBP
796 Inactivation Promotes the Development of HDAC3-Dependent Lymphomas.
797 *Cancer Discov.* American Association for Cancer Research; 2017;7:38–53.
- 798 31. Mondello P, Tadros S, Teater M, Fontán L, Chang AY, Jain N, et al. Selective
799 Inhibition of HDAC3 Targets Synthetic Vulnerabilities and Activates Immune
800 Surveillance in Lymphoma. *Cancer Discov.* American Association for Cancer
801 Research; 2020;10:440–59.
- 802 32. Knutson SK, Kawano S, Minoshima Y, Warholc NM, Huang K-C, Xiao Y, et
803 al. Selective inhibition of EZH2 by EPZ-6438 leads to potent antitumor activity
804 in EZH2-mutant non-Hodgkin lymphoma. *Mol Cancer Ther.* American
805 Association for Cancer Research; 2014;13:842–54.
- 806 33. McCabe MT, Ott HM, Ganji G, Korenchuk S, Thompson C, Van Aller GS, et al.
807 EZH2 inhibition as a therapeutic strategy for lymphoma with EZH2-activating
808 mutations. *Nature.* Nature Publishing Group; 2012;492:108–12.
- 809 34. Yuan CC, Jeon AJ, Tucker-Kellogg G, Bryant B, 2019. EZH2 inhibition results
810 in genome-wide PRC2 redistribution. *bioRxiv.*
- 811 35. Khalil AM, Cambier JC, Shlomchik MJ. B cell receptor signal transduction in
812 the GC is short-circuited by high phosphatase activity. *Science.* 2012;336:1178–
813 81.
- 814 36. Rickert RC. New insights into pre-BCR and BCR signalling with relevance to B
815 cell malignancies. *Nature reviews Immunology.* Nature Publishing Group;
816 2013;13:578–91.

- 817 37. Oka T, Ouchida M, Koyama M, Ogama Y, Takada S, Nakatani Y, et al. Gene
818 silencing of the tyrosine phosphatase SHP1 gene by aberrant methylation in
819 leukemias/lymphomas. *Cancer research*. 2002;62:6390–4.
- 820 38. Havranek O, Xu J, Köhrer S, Wang Z, Becker L, Comer JM, et al. Tonic B-cell
821 receptor signaling in diffuse large B-cell lymphoma. *Blood*. American Society of
822 Hematology; 2017;130:995–1006.
- 823 39. Kinetics of B Cell Receptor Signaling in Human B Cell Subsets Mapped by
824 Phosphospecific Flow Cytometry. *Journal of immunology*. American
825 Association of Immunologists; 2006;177:1581–9.
- 826 40. Davids MS, Roberts AW, Seymour JF, Pagel JM, Kahl BS, Wierda WG, et al.
827 Phase I First-in-Human Study of Venetoclax in Patients With Relapsed or
828 Refractory Non-Hodgkin Lymphoma. *J Clin Oncol*. 2017;35:826–33.
- 829 41. Kotschy A, Szlavik Z, Murray J, Davidson J, Maragno AL, Le Toumelin-Braizat
830 G, et al. The MCL1 inhibitor S63845 is tolerable and effective in diverse cancer
831 models. *Nature*. Nature Publishing Group; 2016;538:477–82.
- 832 42. Bartlett NL, Costello BA, LaPlant BR, Ansell SM, Kuruvilla JG, Reeder CB, et
833 al. Single-agent ibrutinib in relapsed or refractory follicular lymphoma: a phase 2
834 consortium trial. *Blood*. American Society of Hematology; 2018;131:182–90.
- 835 43. Cao J, Wu L, Zhang S-M, Lu M, Cheung WKC, Cai W, et al. An easy and
836 efficient inducible CRISPR/Cas9 platform with improved specificity for multiple
837 gene targeting. *Nucleic acids research*. 2016;44:e149.
- 838 44. Brier A-SB, Loft A, Madsen JGS, Rosengren T, Nielsen R, Schmidt SF, et al.
839 The KDM5 family is required for activation of pro-proliferative cell cycle genes
840 during adipocyte differentiation. *Nucleic acids research*. 2017;45:1743–59.
- 841 45. Li J, Yu B, Deng P, Cheng Y, Yu Y, Kevork K, et al. KDM3 epigenetically
842 controls tumorigenic potentials of human colorectal cancer stem cells through
843 Wnt/ β -catenin signalling. *Nat Comms*. Nature Publishing Group; 2017;8:3286.
- 844 46. Pedersen MT, Kooistra SM, Radziszewska A, Laugesen A, Johansen JV,
845 Hayward DG, et al. Continual removal of H3K9 promoter methylation by Jmjd2
846 demethylases is vital for ESC self-renewal and early development. *EMBO J*.
847 John Wiley & Sons, Ltd; 2016;35:1550–64.
- 848 47. García-Ramírez I, Tadros S, González-Herrero I, Martín-Lorenzo A, Rodríguez-
849 Hernández G, Moore D, et al. Crebbp loss cooperates with Bcl2 overexpression
850 to promote lymphoma in mice. *Blood*. American Society of Hematology;
851 2017;129:2645–56.
- 852 48. Horton SJ, Giotopoulos G, Yun H, Vohra S, Sheppard O, Bashford-Rogers R, et
853 al. Early loss of Crebbp confers malignant stem cell properties on lymphoid
854 progenitors. *Nat Cell Biol*. Nature Publishing Group; 2017;19:1093–104.
- 855 49. Hashwah H, Schmid CA, Kasser S, Bertram K, Stelling A, Manz MG, et al.
856 Inactivation of CREBBP expands the germinal center B cell compartment, down-
857 regulates MHCII expression and promotes DLBCL growth. *Proceedings of the*
858 *National Academy of Sciences*. National Acad Sciences; 2017;114:9701–6.

- 859 50. Béguelin W, Popovic R, Teater M, Jiang Y, Bunting KL, Rosen M, et al. EZH2
860 Is Required for Germinal Center Formation and Somatic EZH2 Mutations
861 Promote Lymphoid Transformation. *Cancer Cell*. Elsevier; 2013;23:677–92.
- 862 51. Velichutina I, Shaknovich R, Geng H, Johnson NA, Gascoyne RD, Melnick AM,
863 et al. EZH2-mediated epigenetic silencing in germinal center B cells contributes
864 to proliferation and lymphomagenesis. *Blood*. American Society of Hematology;
865 2010;116:5247–55.
- 866 52. Bödör C, Grossmann V, Popov N, Okosun J, O'Riain C, Tan K, et al. EZH2
867 mutations are frequent and represent an early event in follicular lymphoma.
868 *Blood*. American Society of Hematology; 2013;122:3165–8.
- 869 53. Morschhauser F, Salles G, McKay P, Tilly H, schmitt A, Gerecitano J, et al.
870 Interim report from a phase 2 multicenter study of tazemostat, an EZH2
871 inhibitor: clinical activity and favourable safety in patients with relapsed or
872 refractory B-cell non-hodgkin lymphoma. *International Conference on Malignant
873 Lymphoma*. 2017 Jun.
- 874 54. Knutson SK, Wigle TJ, Warholic NM, Sneeringer CJ, Allain CJ, Klaus CR, et al.
875 A selective inhibitor of EZH2 blocks H3K27 methylation and kills mutant
876 lymphoma cells. *Nat Chem Biol*. Nature Publishing Group; 2012;8:890–6.
- 877 55. Souers AJ, Levenson JD, Boghaert ER, Ackler SL, Catron ND, Chen J, et al.
878 ABT-199, a potent and selective BCL-2 inhibitor, achieves antitumor activity
879 while sparing platelets. *Nature medicine*. Nature Publishing Group;
880 2013;19:202–8.
- 881 56. Klanova M, Andera L, Brazina J, Svadlenka J, Benesova S, Soukup J, et al.
882 Targeting of BCL2 Family Proteins with ABT-199 and Homoharringtonine
883 Reveals BCL2- and MCL1-Dependent Subgroups of Diffuse Large B-Cell
884 Lymphoma. *Clin Cancer Res*. American Association for Cancer Research;
885 2016;22:1138–49.
- 886 57. Hatzi K, Geng H, Doane AS, Meydan C, LaRiviere R, Cardenas M, et al.
887 Histone demethylase LSD1 is required for germinal center formation and BCL6-
888 driven lymphomagenesis. *Nature immunology*. Nature Publishing Group;
889 2019;20:86–96.
- 890 58. Ramírez F, Ryan DP, Grüning B, Bhardwaj V, Kilpert F, Richter AS, et al.
891 deepTools2: a next generation web server for deep-sequencing data analysis.
892 *Nucleic acids research*. 2016;44:W160–5.

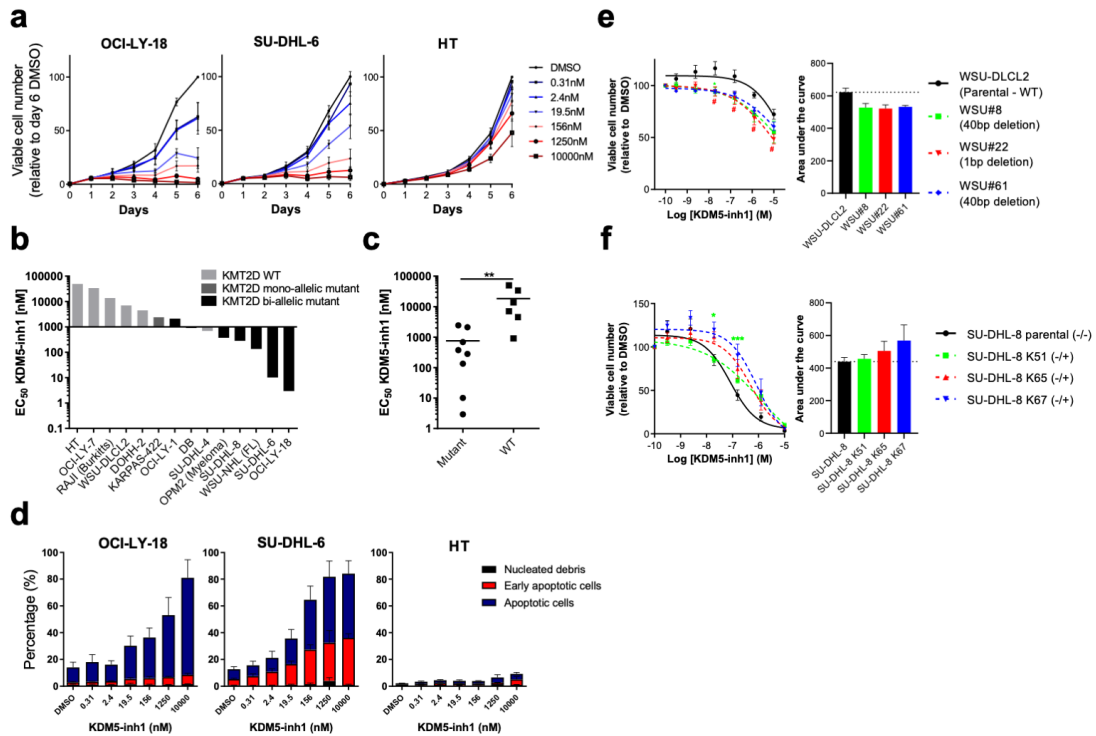
893
894
895
896
897

898 **Figures:**
899



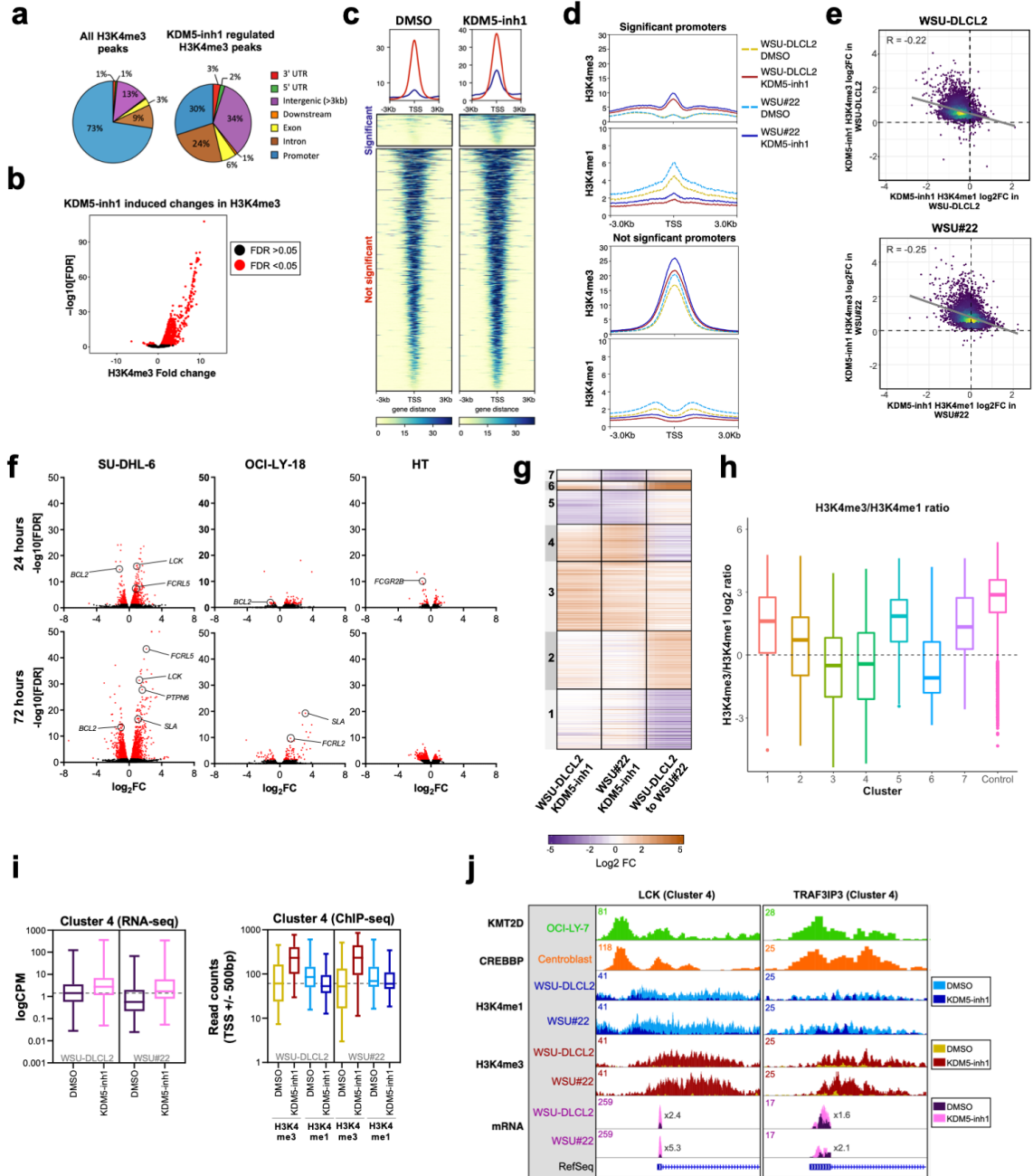
900

901 **Figure 1. KDM5-inhibition increases H3K4me3 levels in DLBCL cell lines.** (a) The
902 expression of the four *KDM5* family members (*KDM5A-D*) was examined by qRT-PCR in 10
903 DLBCL cell lines and normalised to the expression of GAPDH. Data are the mean \pm SEM of
904 three independent experiments. (b) *KDM5* family member expression was examined by RNA-
905 seq in publicly available datasets of FL (ICGC, n=97 (21)) and DLBCL (TCGA n=48, ICGC
906 n=74) patients, plus healthy GC B-cells (BLUEPRINT (22)). RPKM = Reads Per Kilobase
907 Million, TPM = Transcripts Per Million. (c) SU-DHL-6 cells were treated with 1 μ M *KDM5*-
908 inh1 or 10 μ M Compound-48 and *KDM5*-C70 for 48h, 72h and 96h, followed by western blot
909 analysis of H3K4me3 levels relative to H3. The SU-DHL-6 cell line was (d) treated with
910 DMSO or 1 μ M *KDM5*-inh1 for increasing lengths of time and (e) for 48h with DMSO or
911 increasing concentrations of *KDM5*-inh1. The upper panels display representative western
912 blots for H3K4me3/me2/me1 and H3. The lower panel displays the quantification of western
913 blots relative to H3. Data are the mean \pm SEM of 3 independent experiments. Statistical
914 significance was determined using an ANOVA with a Dunnett's post-test versus untreated
915 control, where * P<0.05 and ** P<0.01.



916

917 **Figure 2. KDM5-inhibition reduces the proliferation of *KMT2D* mutant cell lines.** DLBCL,
 918 FL, myeloma and Burkitt's lymphoma cell lines were treated with DMSO or increasing
 919 concentrations of KDM5-inh1, and viable cells quantified **(a)** every day up to 6 days for OCI-
 920 LY-18, SU-DHL-6 and HT cells **(b)** and after 5 days for all cell lines, with EC₅₀ values for
 921 *KMT2D* WT and mutant cell lines displayed in a waterfall plot. **(c)** Dot plot showing the
 922 significantly lower EC₅₀ values for *KMT2D* mutant cell lines. Statistical significance was
 923 determined by Mann Whitney U test, where ** P<0.01. **(d)** Induction of apoptosis was
 924 quantified in OCI-LY-18, SU-DHL-6 and HT cells treated with DMSO or increasing
 925 concentrations KDM5-inh1 for 5 days. Viable cell counts from **(e)** WSU-DLCL2 cells and 3
 926 *KMT2D* mutant clones or **(f)** parental SU-DHL-8 cells and 3 corrected clones treated with
 927 DMSO or increasing concentrations of KDM5-inh1 for 5 days. Data are the mean ± SEM of 3-
 928 7 independent experiments. Statistical significance was calculated using a two-way ANOVA
 929 with a Dunnett's post-test, where */# P < 0.005 and *** P < 0.001.

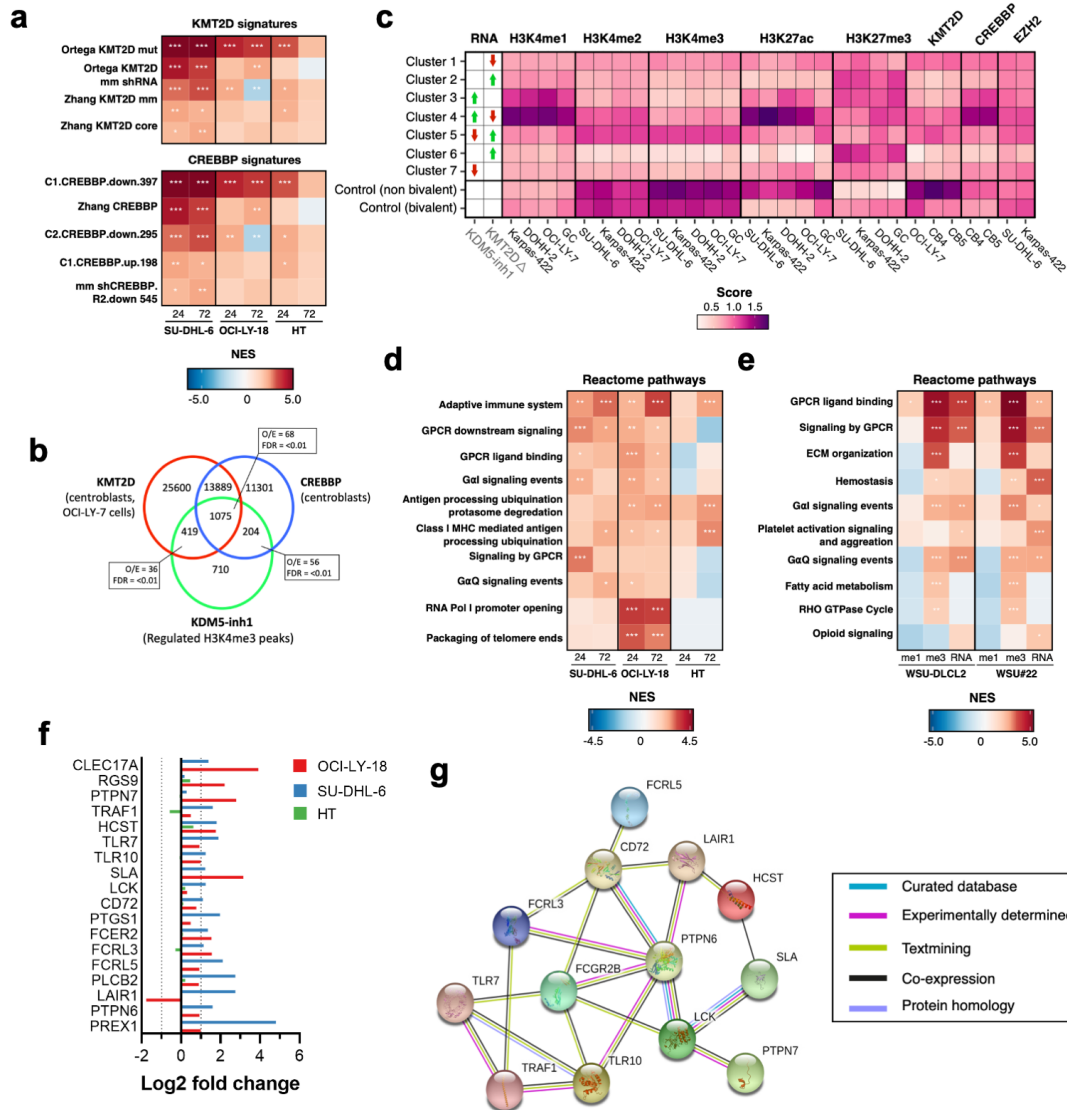


930

931

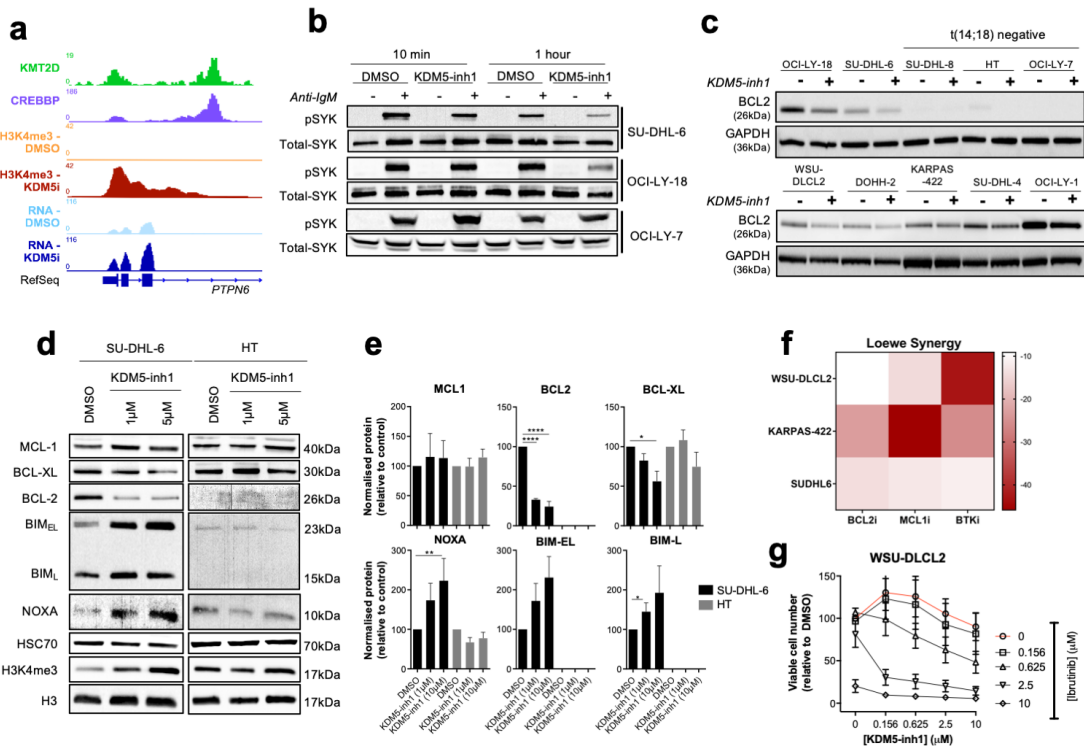
932

933 **Figure 3. Epigenetic and transcriptomic characterisation of KDM5-inhibition. (a)**
934 Genomic locations of H3K4me3 peaks identified by ChIP-seq in cells treated with DMSO (left)
935 or 1 μ M KDM5-inh1 (right) for 72h. **(b)** KDM5-inhibition induced changes in H3K4me3, with
936 significantly changed peaks displayed in red. **(c)** Heatmaps of ChIP-seq data showing
937 difference in H3K4me3 levels between promoters significantly altered (blue) or otherwise (red)
938 in SU-DHL-6 cells treated with DMSO or 1 μ M KDM5-inh1 for 72h. **(d)** Spatial plots showing
939 distribution of H3K4me1 and H3K4me3 at promoters with significantly altered H3K4me3 by
940 KDM5-inh1 or otherwise, in WSU-DLCL2 (yellow/red) and WSU#22^{-/+} (light/dark blue) cells
941 treated with DMSO (yellow/light blue) or KDM5-inh1 (red/dark blue). **(e)** Plots showing broad
942 increases in H3K4me3 and reductions in H3K4me1, quantified by ChIP-seq, at the TSS (+/-
943 500bp) of H3K4me3⁺ genes in WSU-DLCL2 and WSU#22^{-/+} cells treated with 1 μ M KDM5-
944 inh1. The Pearson's correlation co-efficient is indicated on each plot. **(f)** Volcano plots
945 indicating DE genes in SU-DHL-6, OCI-LY-18 and HT cells treated with 1 μ M KDM5-inh1
946 for 24h and 72h, with significant genes highlighted in red. **(g)** Heatmap showing log₂FC values
947 for 897 genes that were DE by either KDM5-inh1 or *KMT2D* loss, and clustered using K-means
948 clustering. **(h)** H3K4me3 and H3K4me1 reads were counted for the promoters in each cluster,
949 then divided (H3K4me3/H3K4me1) and log₂ normalised to create a summary ratio for each.
950 Control promoters were identified as being H3K4me3⁺ in WSU-DLCL2 cells but showing no
951 alteration in mRNA expression or H3K4me3/H3K4me1 deposition in any of our analyses. **(i)**
952 Boxplots showing RNA-seq logCPM values (left) and TSS read counts across ChIP-seq (right)
953 datasets, of genes from Cluster Four. **(j)** ChIP-seq and RNA-seq tracks, centred on *LCK* and
954 *TRAF3IP3*, from WSU-DLCL2 and WSU#22^{-/+} cells treated with KDM5-inh1 for 72h, plus
955 ChIP-seq tracks of KMT2D (OCI-LY-7) (9) and CREBBP (centroblasts) (29) binding.



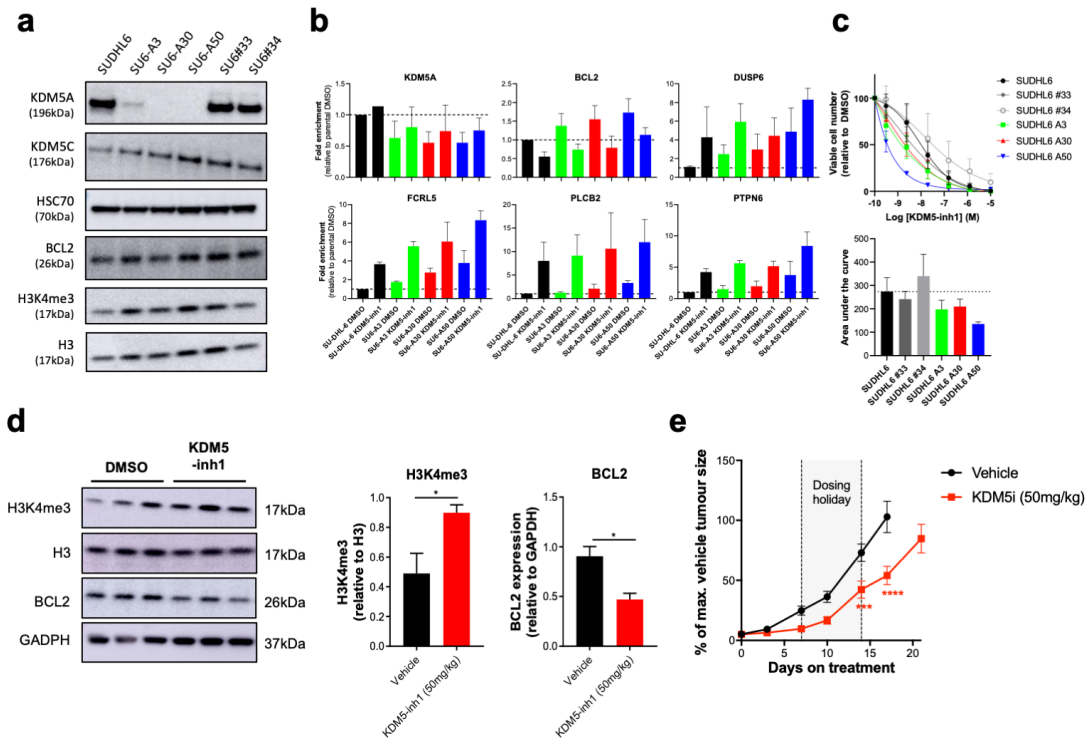
956

957 **Figure 4. KDM5-inhibition regulates KMT2D target genes and BCR-signalling**
 958 **regulators. (a)** Heatmap indicating normalized enrichment scores (NES) of KMT2D and
 959 CREBBP signatures in KDM5-inh1 treated cells, following GSEA of RNA-seq profiles using
 960 a manually curated database of B-cell signatures. **(b)** Overlap between KDM5-inhibition
 961 regulated regions in SU-DHL-6 and CREBBP (29) or KMT2D bound regions (9,10), with
 962 observed/expected and FDR values for the overlaps indicated. **(c)** DeepTools (58) was used
 963 to calculate summary scores at the promoters (TSS \pm 500bp) of genes in each cluster (Figure 3f),
 964 plus non-bivalent (H3K4me3+/H3K27me3-) and bivalent (H3K4me3/H3K27me3+) control
 965 promoters, for ChIP-seq datasets of histone mark deposition (ENCODE/BLUEPRINT) and
 966 KMT2D (9,10), CREBBP (29) and EZH2/SUZH12 (34) binding. The overall direction of
 967 change in RNA expression, following KDM5i or *KMT2D* loss, is indicated for each cluster in
 968 the first two columns. **(d+e)** Heatmaps indicating NES following GSEA of the Reactome
 969 database in **(d)** RNA-seq profiles from KDM5-inh1 treated cells and **(e)** RNA-seq plus
 970 promoter H3K4me1 and H3K4me3 profiles from KDM5-inh1 treated WSU-DLCL2/WSU#22^{+/+}
 971 cells. **(f)** Log₂FC values of BCR-signalling regulators in SU-DHL-6, OCI-LY-18 and HT
 972 cells treated with KDM5-inh1. **(g)** String analysis (<https://string-db.org/>) showing the
 973 interaction network of identified BCR-signalling regulators.



974

975 **Figure 5. KDM5-inhibition alters the expression of BCR-signalling and apoptotic**
 976 **regulatory genes. (a)** ChIP-seq and RNA-seq tracks, centred on the *PTPN6* promoter, from
 977 SU-DHL-6 cells treated with DMSO or 1 μ M KDM5-inh1 for 72h, plus ChIP-seq tracks of
 978 KMT2D (9) and CREBBP (29) binding in GC centroblasts. **(b)** Activation of the BCR-
 979 associated kinase SYK was investigated by western blot analysis in SU-DHL-6, OCI-LY-18
 980 and OCI-LY-7 cells treated with DMSO or KDM5-inh1 for 72h, followed by anti-IgM F(ab')₂
 981 antibody stimulation for 10 min or 1h. **(c)** Expression of BCL2 protein was examined by
 982 western blot in 10 DLBCL cell lines exposed to DMSO or 1 μ M KDM5-inh1 48h. **(d)** SU-DHL-
 983 6 and HT cells were treated with DMSO or 1 μ M and 5 μ M KDM5-inh1 for 5 days, with the
 984 cells re-seeded in fresh drug/media after 48h. The expression of BCL2 family members was
 985 investigated by western blot, with HSC70 used as a loading control. Western blots are
 986 representative of 3 independent experiments, with the quantification relative to HSC70
 987 displayed in **(e)**. Statistical significance was determined using an ANOVA with a Dunnett's
 988 post-test versus untreated control, where * P<0.05, ** P<0.01 and **** P < 0.0001. **(f)** SU-
 989 DHL-6, KARPAS-422 and WSU-DLCL2 cells were treated with increasing concentrations of
 990 KDM5-inh1 for 5 days, alongside increasing concentrations of S63845 (MCL1i), Venetoclax
 991 (BCL2i) for 2 days or Ibrutinib (BTKi) for 3 days. Viable cells were quantified and an overall
 992 Loewe synergy score calculated for each combination. **(g)** Plot showing viable cell numbers
 993 following KDM5-inh1 and Ibrutinib combinations in WSU-DLCL2 cells. Data are the mean \pm
 994 SEM of 3 independent experiments.



995

996 **Figure 6. KDM5-inhibition likely acts through multiple isoforms and is efficacious *in vivo*.**
 997 **(a)** Western blot showing loss of KDM5A in three homozygous knockout clones (SU6-A3,
 998 A30, A50) compared to parental and WT controls (SU6#33, #34), alongside expression of
 999 KDM5C, BCL2 and H3K4me3 levels. **(b)** qRT-PCR analysis of *KDM5A* and KDM5-inhibition
 1000 target genes in SU-DHL-6 and KDM5A knockout clones exposed to DMSO or 1 μ M KDM5-
 1001 inh1 for 72h. Data are the mean \pm SEM of two independent experiments. **(c)** SU-DHL-6 and
 1002 KDM5A knockout clones were exposed to DMSO or increasing concentrations of KDM5-inh1
 1003 for five days, and viable cell numbers quantified. Concentration response curves are shown in
 1004 the upper panel and AUC values in the lower panel. Data are the mean \pm SEM of three
 1005 independent experiments. **(d)** Global levels of H3K4me3 in tumours from mice treated with
 1006 vehicle or 50mg/kg KDM5-inh1 for 1 week (n=3) were quantified by western blot and
 1007 normalised to H3, whilst BCL2 levels were quantified and normalised to GAPDH.
 1008 Quantification of the western blots is displayed on the right-hand side. **(e)** Activity of 50mg/kg
 1009 KDM5-inh1 on the growth of SU-DHL-6 xenografts, in comparison to vehicle treated mice.
 1010 Data are the mean \pm SEM of 10 individual mice, except in the vehicle group where one mouse
 1011 was removed due to insufficient tumour growth (<300mm³). Statistical significance was
 1012 calculated using a two-way ANOVA with a Dunnett's post-test, where *** P < 0.001 and ****
 1013 P < 0.0001.

1014

1015

1016

1017